## Journal of Materials Chemistry C



**PAPER** 

View Article Online



Cite this: J. Mater. Chem. C, 2021, 9, 9251

# properties of two methylammonium silver halides: CH<sub>3</sub>NH<sub>3</sub>AgBr<sub>2</sub> and CH<sub>3</sub>NH<sub>3</sub>Ag<sub>2</sub>I<sub>3</sub>†

Synthesis, crystal chemistry, and optical

Matthew B. Gray, D Noah P. Holzapfel, D Tianyu Liu, D Victor da Cruz Pinha Barbosa, D Nicholas P. Harvey and Patrick M. Woodward D\*

Two novel ternary compounds from the pseudobinary  $CH_3NH_3X-AgX$  (X = Br, I) phase diagrams are reported.  $CH_3NH_3AgBr_2$  and  $CH_3NH_3Ag_2l_3$  were synthesized via solid state sealed tube reactions and the crystal structures were determined through a combination of single crystal and synchrotron X-ray powder diffraction. Structurally, both compounds consist of one-dimensional ribbons built from silvercentered tetrahedra. The structure of CH3NH3AgBr2 possesses orthorhombic Pnma symmetry and is made up of zig-zag chains where each silver bromide tetrahedron shares two edges with neighboring tetrahedra. The tetrahedral coordination of silver is retained in  $CH_3NH_3Aq_2I_3$ , which has monoclinic  $P2_1/m$ symmetry, but the change in stoichiometry leads to a greater degree of edge-sharing connectivity within the silver iodide chains. With band gaps of 3.3 eV (CH<sub>3</sub>NH<sub>3</sub>Aq<sub>2</sub>I<sub>3</sub>) and 4.0 eV (CH<sub>3</sub>NH<sub>3</sub>AqBr<sub>2</sub>) the absorption onsets of the ternary phases are significantly blue shifted from the binary silver halides, AgBr and Agl, due in part to the decrease in electronic dimensionality. The compounds are stable for at least one month under ambient conditions and are thermally stable up to approximately 200 °C. Density functional theory calculations reveal very narrow valence bands and moderately disperse conduction bands with Aq 5s character. Bond valence calculations are used to analyze the hydrogen bonding between methylammonium cations and coordinatively unsaturated halide ions. The crystal chemistry of these compounds helps to explain the dearth of iodide double perovskites in the literature.

Received 14th April 2021, Accepted 2nd June 2021

DOI: 10.1039/d1tc01737c

rsc.li/materials-c

## Introduction

Recent photovoltaic research has shown that perovskite films, namely  $APbI_{3-x}Br_x$  (A =  $CH_3NH_3^+$ ,  $CH(NH_2)_2^+$  (FA<sup>+</sup>),  $Cs^+$ ), are fast approaching efficiencies that can compete with existing siliconbased technologies. However, concerns about the toxicity of lead persist. One proposed method to reduce the toxicity of these devices without reducing efficiency is to replace simple perovskite absorbers, APbX<sub>3</sub>, with double perovskites, A<sub>2</sub>MM'X<sub>6</sub>  $(X = Br^-, I^-)$ , where M and M' are a combination of cations with an overall 4+ charge.<sup>2,3</sup> Calculations have shown that the most suitable M' cations to replace Pb2+ are Bi3+ and Sb3+, as they both contain an ns<sup>2</sup> electronic configuration like Pb<sup>2+</sup>.<sup>4</sup> Choosing an appropriate M<sup>+</sup> cation is less straightforward; In<sup>+</sup> and Tl<sup>+</sup> have the correct electronic configurations,<sup>5</sup> but In<sup>+</sup> is oxidatively unstable and Tl<sup>+</sup> is toxic. The most commonly used

Department of Chemistry and Biochemistry, The Ohio State University, 100 W. 18th Avenue, Columbus, Ohio 43210, USA. E-mail: woodward.55@osu.edu † Electronic supplementary information (ESI) available. CCDC 2076542 and 2076543. For ESI and crystallographic data in CIF or other electronic format see DOI: 10.1039/d1tc01737c

1+ cation in semiconducting halide double perovskite is Ag<sup>+</sup>, as the filled 4d orbitals contribute to states near the valence band maximum which typically leads to a small reduction in

Unfortunately, attempts to coax Ag<sup>+</sup> into an octahedral coordination environment in bromide and iodide perovskites have met with limited success. A few silver bromide double perovskites have been reported: Cs2AgBiBr6, Cs2AgSbBr6, Cs<sub>2</sub>AgTlBr<sub>6</sub>, and (CH<sub>3</sub>NH<sub>3</sub>)<sub>2</sub>AgBiBr<sub>6</sub>. There are two bulk silver iodide double perovskites reported: (CH3NH3)2AgSbI6 and (CH<sub>3</sub>NH<sub>3</sub>)<sub>2</sub>AgBiI<sub>6</sub>. 12,13 However, the existence of these compositions is somewhat questionable because their PXRD patterns are uncharacteristically complex for the cubic (or nearly cubic) double perovskite structure.

Replacing Cs<sup>+</sup> with a small organic cation like methylammonium could allow three-dimensional iodide double perovskites to be stabilized. However, synthetic attempts by our group and others have shown limited stability of (CH3NH3)2MM'X6 (X = Br<sup>-</sup>, I<sup>-</sup>) double perovskites; only bromides have been reported, and those systems are typically phase mixtures. 11,14,15 Larger organic cations cause a dimensional reduction which has been shown to stabilize six-coordinate silver iodide polyhedra, but

the silver coordination environment tends to be heavily distorted and might alternatively be described as linear, a coordination environment not uncommon for cations with a d10 electron configuration, like Ag<sup>+</sup>. <sup>16-18</sup> For example, in (C<sub>3</sub>H<sub>9</sub>NI)<sub>4</sub>AgBiI<sub>8</sub> the silver iodide bond lengths are 2  $\times$  2.6915(9) Å and 4  $\times$  3.4176(9) Å.<sup>17</sup> In compounds like (5,5'-diylbis(aminoethyl)-[2,2'-bithiophene])<sub>4</sub>AgBiI<sub>8</sub>, where the Ag<sup>+</sup> and Bi<sup>3+</sup> are disordered on the same crystallographic site, the exact nature of the local silver coordination environment is obscured by the disorder.19

Here we explore the pseudobinary  $CH_3NH_3X-AgX$  (X = Br<sup>-</sup>, I<sup>-</sup>) phase diagrams and describe the characteristics of two new ternary compounds: CH<sub>3</sub>NH<sub>3</sub>AgBr<sub>2</sub> and CH<sub>3</sub>NH<sub>3</sub>Ag<sub>2</sub>I<sub>3</sub>. The halide coordination environment of silver is tetrahedral in both compounds, a review of the literature shows that this coordination environment is strongly favored in ternary silver halides. Prior reports of methylammonium silver iodide double perovskites are reexamined and determined to be phase mixtures. The optical properties of CH3NH3AgBr2 and CH3NH3Ag2I3 are indicative of wide band gap semiconductors, and band structure calculations confirm the pseudo one-dimensional electronic structure.

## **Experimental**

AgBr (Alfa Aesar, 99.5%) and AgI (Alfa Aesar, 99.9%) were purchased and used as received. CH<sub>3</sub>NH<sub>3</sub>Br and CH<sub>3</sub>NH<sub>3</sub>I were synthesized by the neutralization of methylamine (40 wt% in  $H_2O$ , Sigma-Aldrich) with either HBr (Sigma Aldrich,  $\geq 47\%$ ) or HI (Sigma-Aldrich,  $\geq 47.0\%$ , with < 1.5% H<sub>3</sub>PO<sub>2</sub>) in cold ethanol (Deacon Labs, 200 proof). The resulting white powders were ground and transferred to a glass vial, which was placed under vacuum overnight. Typical yields were >90%. After preparation, the salts were stored in a desiccator until use.

CH<sub>3</sub>NH<sub>3</sub>AgBr<sub>2</sub> and CH<sub>3</sub>NH<sub>3</sub>Ag<sub>2</sub>I<sub>3</sub> were synthesized via solid state reactions in evacuated silica ampoules. For a typical 1.50 g synthesis, stoichiometric ratios of the binary halide salts (CH<sub>3</sub>NH<sub>3</sub>Br + AgBr or CH<sub>3</sub>NH<sub>3</sub>I + 2AgI) were ground in air for 15 minutes in an agate mortar and pestle and then loaded into a silica ampoule (9 mm ID  $\times$  13 mm OD, Technical Glass Products) and placed under dynamic vacuum on a Schlenk line at  $\sim 50$  mTorr for 10 minutes before sealing with an  $H_2/O_2$ torch. The sealed ampoules were then annealed for three heating cycles at 125 °C for 72 hours tilted at a 45° angle in a box furnace. Between each heating cycle the samples were cooled back to room temperature, the ampoule was opened and the sample ground in a mortar and pestle before resealing in an evacuated ampoule.

Crystals suitable for single crystal diffraction were synthesized via solvothermal methods. For CH3NH3AgBr2, 3 mL of acetonitrile (Fisher Scientific, 99.9%) and 1.67 mmol of CH<sub>3</sub>NH<sub>3</sub>Br (0.1868 g) and 1.67 mmol of AgBr (0.3132 g) were placed in a Teflon-lined Parr reactor. The vessel was sealed and heated in a box furnace to 120 °C for 10 hours before cooling at 3 °C h<sup>-1</sup> to 25 °C. Single crystals of CH<sub>3</sub>NH<sub>3</sub>AgBr<sub>2</sub> were filtered and washed with diethyl ether (Fisher Scientific). A similar procedure was used to grow crystals of CH3NH3Ag2I3, however,

methanol (10 mL, Fisher Scientific, 99.9%) was used as the solvent and the maximum temperature was reduced to 100 °C (0.5 g scale).

Attempted syntheses of (CH<sub>3</sub>NH<sub>3</sub>)<sub>2</sub>AgSbI<sub>6</sub> and (CH<sub>3</sub>NH<sub>3</sub>)<sub>2</sub> AgBiI<sub>6</sub> followed the reported synthetic procedures. <sup>12,13</sup> CH<sub>3</sub>NH<sub>3</sub>I, AgI, and either SbI<sub>3</sub> (Sigma Aldrich, 98%+) or BiI<sub>3</sub> (Sigma Aldrich, 99%+) were ground in an argon glove box, evacuated using a Schlenk line, sealed in a quartz ampoule, and heated according to the literature procedure (200 °C, 2 hours).

Powder X-ray diffraction (PXRD) data were collected on a Bruker D8 Advance powder diffractometer (40 kV, 40 mA, sealed Cu X-ray tube) equipped with a Lynxeye XE-T position-sensitive detector. The data were collected with an incident beam monochromator (Johansson type SiO2 crystal) that selects only Cu  $K_{\alpha 1}$  radiation ( $\lambda = 1.5406$  Å). Synchrotron PXRD was collected on the 11-BM beamline at the Advanced Photon Source (APS) with  $\lambda = 0.412748$  Å. Samples were packed into 0.8 mm Kapton tubes and sealed with clay. Rietveld refinements of PXRD data were carried out using the TOPAS-Academic (Version 6) software package to determine the crystal structure.<sup>20</sup> Crystal structure images were generated in Vesta 3.21

Room temperature single-crystal XRD (SCXRD) studies were carried out on a Nonius Kappa diffractometer equipped with a Bruker APEX-II CCD and Mo K $\alpha$  radiation ( $\lambda = 0.71073 \text{ Å}$ ). A  $0.067 \times 0.123 \times 0.451 \text{ mm}^3$  colorless crystal of CH<sub>3</sub>NH<sub>3</sub>AgBr<sub>2</sub>. was mounted on a MiTeGen MicroMount with clear enamel. Data were collected at ambient conditions using  $\varphi$  and  $\omega$  scans. The crystal-to-detector distance was 40 mm, and the exposure time was 7.5 s per frame using a scan width of 0.5°. A total of 2651 reflections were collected covering the indices,  $-10 \le h \le 7$ ,  $-5 \le k \le 4$ ,  $-17 \le l \le 17$ . The number of symmetry independent reflections was 656. For  $CH_3NH_3Ag_2I_3$ , a 0.087  $\times$ 0.109 × 0.183 mm<sup>3</sup> colorless crystal was mounted and data collected in a similar manner. The crystal-to-detector distance was 40 mm, and the exposure time was 10 s per frame using a scan width of 1.0°. A total of 5985 reflections were collected covering the indices,  $-10 \le h \le 10, -7 \le k \le 7, -11 \le l \le 11$ . The number of symmetry independent reflections was 992. For both crystals, the data were integrated using the Bruker SAINT software program and scaled using the SADABS software program. Solution by direct methods (SHELXT) produced a complete phasing model for refinement.<sup>22</sup> All atoms were refined with anisotropic displacement parameters via full-matrix least squares (SHELXL-2014).<sup>23</sup>

UV-visible diffuse reflectance spectra (DRS) were collected from 178 nm to 890 nm with an Ocean Optics USB4000 spectrometer equipped with a Toshiba TCD1304AP (3648-element linear silicon CCD array) detector. The spectrometer features an Ocean Optics DH-2000-BAL deuterium and halogen UVvis-NIR light source and a 400 µm R400-7-ANGLE-vis reflectance probe. The spectrometer was calibrated using a Spectralon Diffuse Reflectance Standard.

Thermogravimetric analysis (TGA) was performed on a TA Instruments TGA 550. Samples were heated under a nitrogen stream of 25 mL min<sup>-1</sup> with a heating rate of 20 °C min<sup>-1</sup> between 25  $^{\circ}\text{C}$  and 575  $^{\circ}\text{C}$ .

Electronic band structure and density of states (DOS) calculations were obtained with density functional theory (DFT)

implemented with the Quantum ESPRESSO (version 6.1) freeware in combination with the BURAI (version 1.3.1) GUI.<sup>24-26</sup> These calculations were performed using projector augmented wave potentials based on the PBE exchange-correlation functional. Cutoff energies of 225.000 Rydberg and a  $4 \times 4 \times 4$ k-point grid were used for both compounds. 28 The calculations did not include spin-orbit coupling.

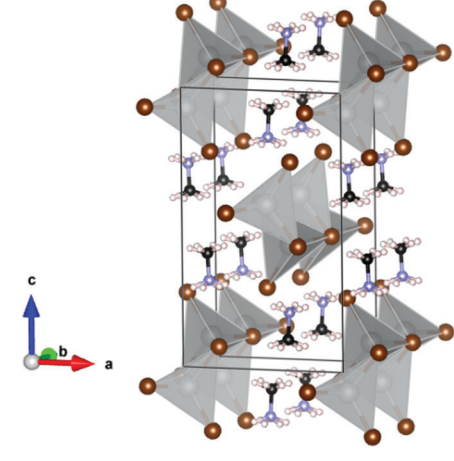
## Results

Solid state syntheses of CH<sub>3</sub>NH<sub>3</sub>AgBr<sub>2</sub> and CH<sub>3</sub>NH<sub>3</sub>Ag<sub>2</sub>I<sub>3</sub> result in off-white crystalline powders. Single crystal growths provide colorless plate-like crystals. For CH<sub>3</sub>NH<sub>3</sub>AgBr<sub>2</sub>, SCXRD data can be fit to the orthorhombic space group Pnma with a = 9.0387(11) Å, b = 4.6831(5) Å, c = 14.7759(13) Å. Details of the resulting crystal structure are provided in Tables S1-S4 (ESI†), and has been deposited in the Cambridge Crystal Structure Database (CCDC 2076542†). This structure, which is shown in Fig. 1, provides a satisfactory fit to the synchrotron PXRD powder data, as seen in the lower half of Fig. 1. The Ag-centered tetrahedron shares two of its six edges with neighboring tetrahedra and contains two chemically distinct bromide ions—one that is shared by three tetrahedra and one that belongs to a single tetrahedron (Niggli formula  $AgBr_{3/3+1/1}$ ). The edge sharing tetrahedra form one-dimensional chains that run parallel to the *b*-axis.

The SCXRD data collected on a crystal of CH3NH3Ag2I3 can be fit to the monoclinic space group  $P2_1/m$  with a = 9.019(3) Å,  $b = 6.329(2) \text{ Å}, c = 9.134(3) \text{ Å}, \beta = 110.431(10)^{\circ}$ . Details of the resulting crystal structure are provided in Tables S1 and S5-S7 (ESI†), and have been deposited in the Cambridge Crystal Structure Database (CCDC 2076543†). This structure, which is shown in Fig. 2, provides a satisfactory fit to the synchrotron PXRD data as illustrated in the lower half of Fig. 2. In this structure, each Ag-centered tetrahedron shares three of its six edges with neighboring tetrahedra to form what might be described as a double chain. In this structure we also see two chemically distinct halide ions, one half of the iodides are shared by four tetrahedra and the other half by two tetrahedra (Niggli formula  $AgI_{2/4+2/2}$ ). The double-chains propagate parallel to the b-axis, and are separated and charge balanced by CH<sub>3</sub>NH<sub>3</sub><sup>+</sup> ions.

CH<sub>3</sub>NH<sub>3</sub>AgBr<sub>2</sub> and CH<sub>3</sub>NH<sub>3</sub>Ag<sub>2</sub>I<sub>3</sub> are stable under ambient light and environmental humidity (~70%). Diffraction measurements taken four weeks apart showed no apparent sample degradation (Fig. S1 and S2, ESI†). The thermal stability of both compounds was assessed via TGA. The decomposition pathway appears to involve loss of CH<sub>3</sub>NH<sub>3</sub>X (X = Br<sup>-</sup>, I<sup>-</sup>), which begins around  $\sim 250$  °C in both compounds (Fig. 3). Mass loss percentages are in good agreement with values that would be expected for complete loss of CH3NH3X.

The optical absorption properties of CH3NH3AgBr2 and CH<sub>3</sub>NH<sub>3</sub>Ag<sub>2</sub>I<sub>3</sub> were measured with UV-vis DRS. The DRS data were transformed using the Kubelka-Munk (KM) function,  $F(R) = (1 - R)^2/2R$ , where F(R) is the optical absorption



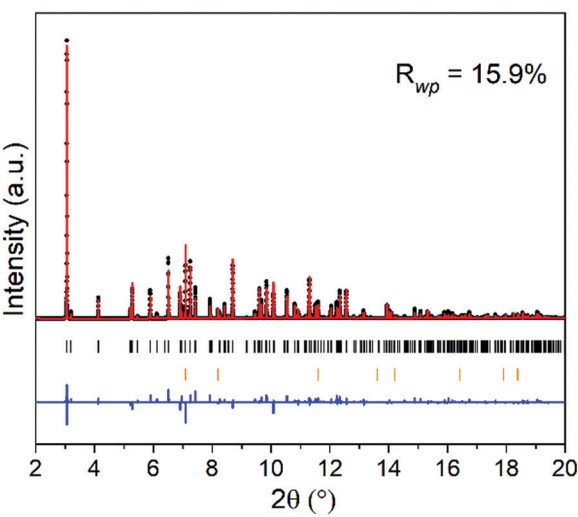


Fig. 1 (top) Crystal structure of CH<sub>3</sub>NH<sub>3</sub>AgBr<sub>2</sub>, showing the positions of Ag (gray), Br (brown), carbon (black), nitrogen (pale blue) and hydrogen (white). The protons of the CH<sub>3</sub>NH<sub>3</sub><sup>+</sup> cations are disordered over two sites. (bottom) The Rietveld fit to synchrotron XRD data taken at 298 K with  $\lambda = 0.412748$  Å. Observed, calculated and difference curves are plotted in black, red and blue, respectively. The expected peak positions for CH<sub>3</sub>NH<sub>3</sub>AgBr<sub>2</sub> are denoted by black tick marks, and those for a AgBr  $(\sim 3\%)$  secondary phase by the lower set of orange tick marks.

coefficient and R is the reflectance. This transformation allows the absorbance of a material to be expressed as a function of the reflectance.<sup>29</sup> Both ternary phases have absorption onsets that are shifted to higher energy (shorter wavelengths) with respect to the corresponding binary silver halide salts (Fig. 4 and Fig. S3, ESI†). The band gaps can be estimated by extrapolating the onset of absorption to the baseline, giving values of 4.0 and 3.3 eV for CH<sub>3</sub>NH<sub>3</sub>AgBr<sub>2</sub> and CH<sub>3</sub>NH<sub>3</sub>Ag<sub>2</sub>I<sub>3</sub>, respectively. The steep rise in absorption seen in both compounds is suggestive of a direct band gap. For CH<sub>3</sub>NH<sub>3</sub>AgBr<sub>2</sub>, the small feature at ~385 nm may be indicative of the AgBr impurity observed in the synchrotron powder diffraction pattern.

Electronic band structure calculations on CH<sub>3</sub>NH<sub>3</sub>AgBr<sub>2</sub> and CH<sub>3</sub>NH<sub>3</sub>Ag<sub>2</sub>I<sub>3</sub> give results that are in reasonable agreement with the DRS measurements (Fig. 5). Due to complications

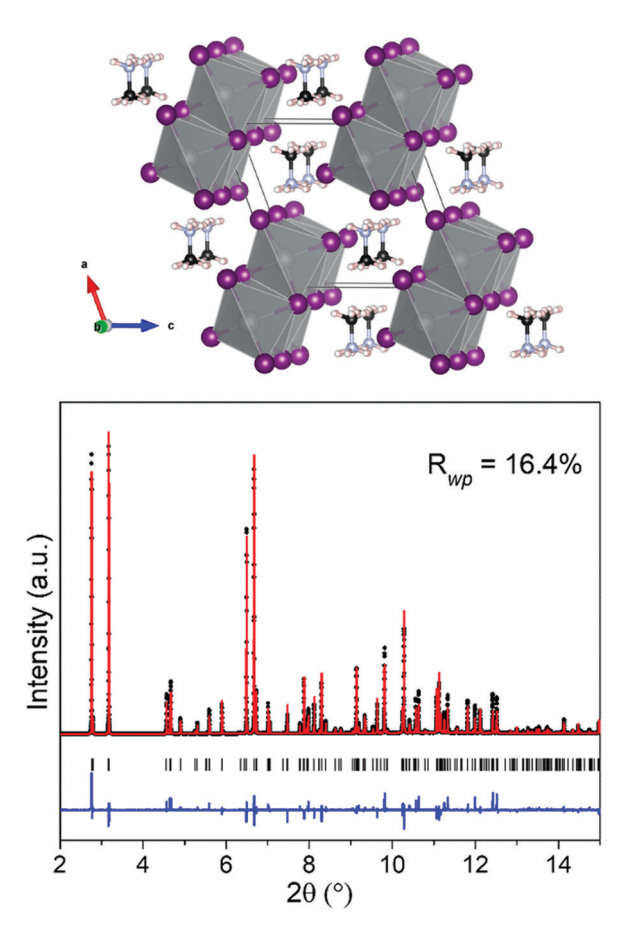


Fig. 2 (top) Crystal structure of CH<sub>3</sub>NH<sub>3</sub>Ag<sub>2</sub>I<sub>3</sub>, showing the positions of Ag (gray), I (purple), carbon (black), nitrogen (pale blue) and hydrogen (white). The protons of the CH<sub>3</sub>NH<sub>3</sub><sup>+</sup> cations are disordered. (bottom) The Rietveld fit to synchrotron XRD data taken at 298 K with  $\lambda$  = 0.412748 Å. Observed, calculated and difference curves are plotted with black, red and blue, respectively. The expected peak positions for CH3NH3Ag2l3 are denoted with black tick marks.

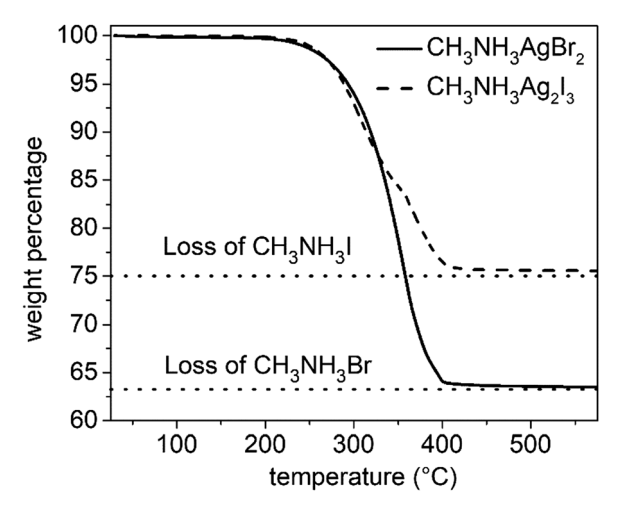


Fig. 3 TGA of  $CH_3NH_3AgBr_2$  and  $CH_3NH_3Ag_2I_3$ . Decomposition began around 250 °C via the loss of the respective methylammonium halide salt.

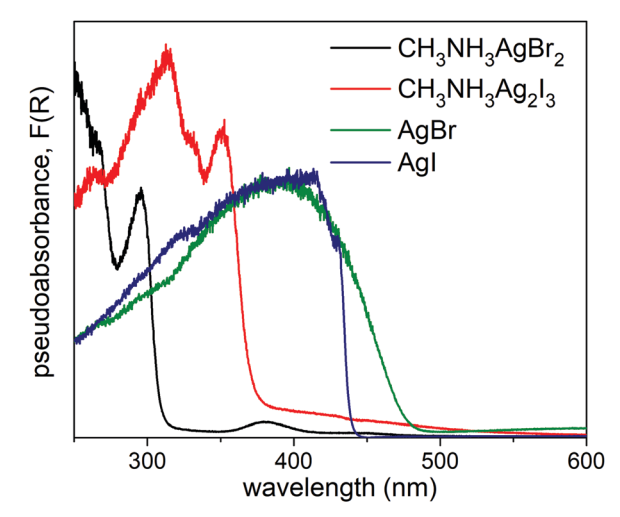


Fig. 4 Kubelka-Munk transformation of the DRS of CH<sub>3</sub>NH<sub>3</sub>AgBr<sub>2</sub> and CH3NH3Ag2l3.

associated with disorder of the hydrogen positions, the CH<sub>3</sub>NH<sub>3</sub><sup>+</sup> was omitted and the calculations were performed on the AgBr<sub>2</sub><sup>-</sup> and Ag<sub>2</sub>I<sub>3</sub><sup>-</sup> charged frameworks. The experimentally determined crystal structures were used without geometric

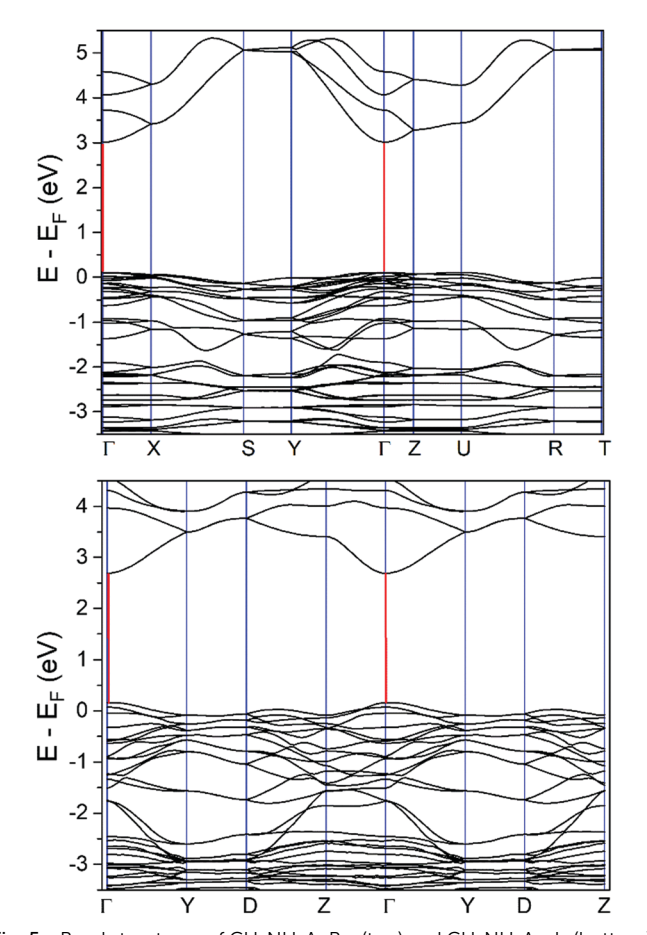


Fig. 5 Band structures of CH<sub>3</sub>NH<sub>3</sub>AgBr<sub>2</sub> (top) and CH<sub>3</sub>NH<sub>3</sub>Ag<sub>2</sub>I<sub>3</sub> (bottom). The lowest energy direct transition occurs at the  $\Gamma$  point in each system, which is highlighted with a red vertical line.

relaxation. This approach is justified as it is generally accepted that CH<sub>3</sub>NH<sub>3</sub><sup>+</sup> does not make significant contributions to the band structure near the Fermi level. Calculated band gaps of 2.9 eV and 2.5 eV for CH<sub>3</sub>NH<sub>3</sub>AgBr<sub>2</sub> and CH<sub>3</sub>NH<sub>3</sub>Ag<sub>2</sub>I<sub>3</sub>, respectively, show a qualitatively similar decrease in the band gap of the iodide compound as observed experimentally. Although, as is often the case, the PBE functionals underestimate the band gap. 30 The calculations confirm a direct transition at the  $\Gamma$ point for both compounds. The frontier valence bands are quite narrow, while the relevant conduction bands are significantly broader, especially for CH<sub>3</sub>NH<sub>3</sub>AgBr<sub>2</sub>. The relative band dispersions for CH<sub>3</sub>NH<sub>3</sub>Ag<sub>2</sub>I<sub>3</sub> are very similar to the results found for CsAg<sub>2</sub>I<sub>3</sub> using the same methodology but leaving the Cs<sup>+</sup> cation in the crystal structure (Fig. S4, ESI†). Calculations including spin-orbit coupling were explored for the CH3NH3Ag2I3 compound (Fig. S5, ESI†). Since there were no major changes in band energies the calculations without spin-orbit coupling are reported here.

DOS calculations reveal the orbital character of the bands near the Fermi level (Fig. 6). As expected, the upper valence bands in both compounds have significant halide-p character, with some admixture of the Ag 4d orbitals. The bands found at bottom of the conduction band arise from antibonding interactions between Ag 5s orbitals and halide-p orbitals. In CH<sub>3</sub>NH<sub>3</sub>AgBr<sub>2</sub> the dispersion of the conduction bands is largest ( $\sim 2.5$  eV) along those directions that are parallel or nearly parallel to the real space *b*-axis (*X*–*S*, *Y*– $\Gamma$ , *U*–*R*), along which the tetrahedra link to form chains. Higher energy conduction bands are primarily Ag-p in character for both compounds, as shown by the DOS. Comparable DOS calculations on CsAg<sub>2</sub>I<sub>3</sub> (Fig. S4, ESI†) are very similar to those for CH<sub>3</sub>NH<sub>3</sub>Ag<sub>2</sub>I<sub>3</sub>.

## Discussion

The space groups, silver coordination environments, and Niggli formulas of the related inorganic A-Ag-X (A = Rb+, Cs+,  $CH_3NH_3^+$ ; X =  $Cl^-$ ,  $Br^-$ ,  $I^-$ ) ternary phases can be found in Table 1. Cell parameters are provided in Table S8 (ESI†). There are two all-inorganic phases with the same silver/halide ratio as CH<sub>3</sub>NH<sub>3</sub>AgBr<sub>2</sub> (CsAgCl<sub>2</sub> and CsAgBr<sub>2</sub>). Interestingly, the silver coordination environments of the all-inorganic and hybrid structures are different. The CsAgX<sub>2</sub> (X = Cl<sup>-</sup>, Br<sup>-</sup>) structures are layered, with the silver cations adopting a distorted square pyramidal environment, with silver having three short bonds ( $\sim 2.7$  Å) and two longer bonds ( $\sim 3.0$  Å). Contrastingly, the CH<sub>3</sub>NH<sub>3</sub>AgBr<sub>2</sub> structure consists of 1-D chains of edge-sharing [AgBr<sub>4</sub>]<sup>3-</sup> tetrahedra with relatively uniform bond lengths of 2.7171(7) Å and 2.6545(11) Å.

Each of the Rb-Ag-X and Cs-Ag-X phase diagrams contain a stable A2AgX3 phase consisting of 1-D chains of cornerconnected [AgX<sub>4</sub>]<sup>3-</sup> tetrahedra. In this orthorhombic structure the ratio of terminal to bridging halide ions is 1:1, a direct consequence of the lack of edge-sharing tetrahedra. Isostructural copper analogs are known for K2CuX3 and Rb2CuX3

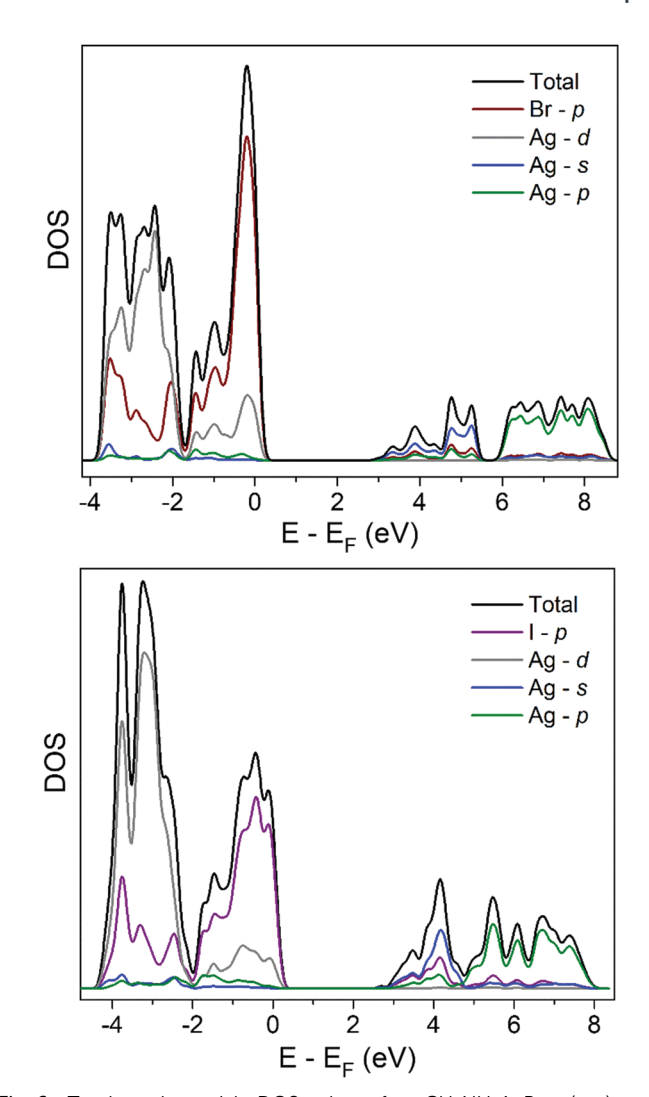


Fig. 6 Total and partial DOS plots for CH<sub>3</sub>NH<sub>3</sub>AgBr<sub>2</sub> (top) and CH<sub>3</sub>NH<sub>3</sub>Ag<sub>2</sub>I<sub>3</sub> (bottom)

 $(X = Cl^-, Br^-)$ , but this structure is not seen for ternary compositions containing the CH<sub>3</sub>NH<sub>3</sub><sup>+</sup> cation.

CH<sub>3</sub>NH<sub>3</sub>Ag<sub>2</sub>I<sub>3</sub> also has an inorganic analogue, CsAg<sub>2</sub>I<sub>3</sub>. The structure of CsAg<sub>2</sub>I<sub>3</sub> consists of a 1-D double-chain of edgesharing tetrahedra very similar to what is found in the  $CH_3NH_3Ag_2I_3$  structure. However, the ordering of the  $CH_3NH_3^+$ cation destroys the b and n-glide planes, which lowers the symmetry from Pbnm to  $P2_1/m$ . An isostructural ternary copper phase, CH<sub>3</sub>NH<sub>3</sub>Cu<sub>2</sub>I<sub>3</sub>, has recently been reported.<sup>35</sup> The different silver coordination environments for the various structures discussed above are depicted in Fig. 7. Bond graphs are shown to emphasize the coordination environments of the halide ions. Increasing the silver to halide ratio necessarily increases the average coordination number of the halide ions.

Bond valence sums (BVS) can be used to gauge the relative stability of all the ions within their coordination environments. The BVS analysis for a variety of ternary silver halides is summarized in Table 2. Revised bond valence parameters for Ag, Cl, Br, and I were used following the methodology suggested by Hull and Berastegui (Appendix A).32 All reported

 $\textbf{Table 1} \quad \text{Space groups, silver coordination environments, and Niggli formulas of ternary } (Rb^+/Cs^+/CH_3NH_3^+) - (Ag^+/Cu^+) - (Cl^-/Br^-/l^-) \text{ phases} \\ \frac{31-33}{1-33} + \frac{31-33}{1$ 

Compound	Space group	Ag/Cu coordination	Niggli formula	Ref.
$Rb_2AgX_3 (X = Cl^-, Br^-, I^-)$	Pnma	Tetrahedron	AgX <sub>2/2+2/1</sub>	31 and 32
$Cs_2AgX_3$ (X = Cl <sup>-</sup> , Br <sup>-</sup> , I <sup>-</sup> )	Pnma	Tetrahedron	$AgX_{2/2+2/1}$	32
$K_2CuX_3$ (X = Cl <sup>-</sup> , Br <sup>-</sup> )	Pnma	Tetrahedron	$AgX_{2/2+2/1}$	32 and 33
$Rb_2CuX_3$ (X = $Cl^-$ , $Br^-$ )	Pnma	Tetrahedron	$AgX_{2/2+2/1}$	32 and 34
$CsAgX_2$ (X = Cl <sup>-</sup> , Br <sup>-</sup> )	Стст	Square pyramid	$AgX_{4/4+1/1}$	32
CH <sub>3</sub> NH <sub>3</sub> AgBr <sub>2</sub>	Pnma	Tetrahedron	$AgBr_{3/3+1/1}$	This work
CsAg <sub>2</sub> I <sub>3</sub>	Pbnm	Tetrahedron	$AgI_{2/4+2/2}$	32
CH <sub>3</sub> NH <sub>3</sub> Cu <sub>2</sub> I <sub>3</sub>	$P2_1/m$	Tetrahedron	CuI <sub>2/4+2/2</sub>	35
$CH_3NH_3Ag_2I_3$	$P2_1/m$	Tetrahedron	$AgI_{2/4+2/2}$	This work
-				

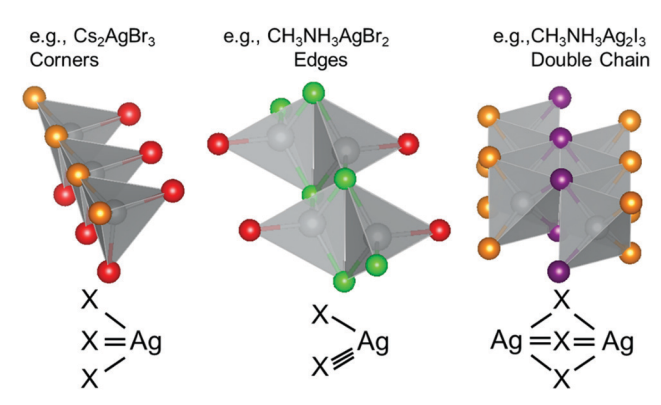


Fig. 7 (top) Silver tetrahedra connectivity for ternary phases with varying silver to halide ratios. The halide ions are color coded by the number of bonds to silver: 1-coordinate (terminal) halide = red, 2-coordinate halide = orange, 3-coordinate halide = green, and 4-coordinate halide = purple. (bottom) Bond graphs, highlighting the halide coordination numbers for each structure type.

inorganic compounds show  $Ag^+$  ions with a BVS between 0.957–1.019 (1 = ideal), except for  $Cs_2AgCl_3$  which has a BVS of 0.757. In the crystal structure of  $Cs_2AgCl_3$ , one Ag–Cl bond is

considerably longer than the others (3.110(1) Å  $\nu s$ . 2.630(1) Å), likely resulting in the low BVS. In the hybrid materials, CH<sub>3</sub>NH<sub>3</sub>AgBr<sub>2</sub> and CH<sub>3</sub>NH<sub>3</sub>Ag<sub>2</sub>I<sub>3</sub>, silver has BVS of 0.985 and 0.966, respectively. This analysis suggests that these two hybrid materials contain tetrahedral environments for Ag<sup>+</sup> that are comparable to those seen in the inorganic compounds.

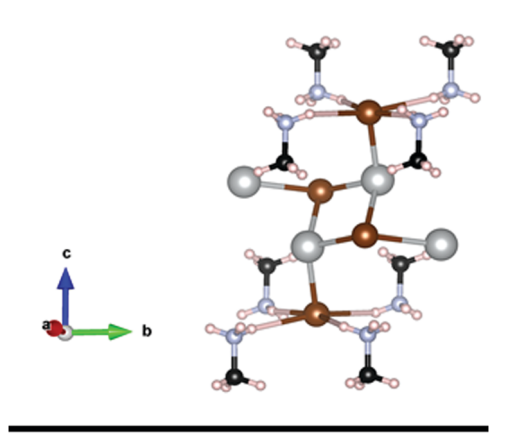
The calculated bond valence sums for the halide ions are all within 10% of the expected value of 1 for the inorganic entries in Table 2, with Cs<sub>2</sub>AgCl<sub>3</sub> once again acting as an outlier. The valences of the bonds between silver and the one-coordinate terminal halides range from 0.236 to 0.320 (excluding Cs<sub>2</sub>AgCl<sub>3</sub>), which means the remaining 70–75% of bond valence must be satisfied by the alkali metal cation, whereas for the 2-coordinate halide ions silver and the alkali metal cation contribute nearly equally to the BVS of the halide ion.

The BVS parameters for the alkali metal–halide ion pairs are well established. However, there are currently no such parameters that exist in the literature to describe the hydrogen bonding interactions between ammonium-type cations (RNH $_3$ ) and the heavier halide ions. Despite this shortcoming, it is clear that a substantial amount of the bonding experienced by the halide ions must come from interactions with the CH $_3$ NH $_3$ + cations. However, the bonding interactions that stabilize the

Table 2 Bond valence sum analysis in the inorganic and hybrid ternary phases. The halide BVS are shown for Ag<sup>+</sup>-only contributions and total BVS

Compound	Ag	A-site		1-Coord.	2-Coord.	3-Coord.	4-Coord.
Rb <sub>2</sub> AgCl <sub>3</sub>	0.999	1.069, 1.092	Ag-only:	0.248, 0.257	0.495	_	_
- 0 -		,	Total:	1.084, 1.094	0.982	_	_
Rb <sub>2</sub> AgBr <sub>3</sub>	1.000	1.035, 1.090	Ag-only:	0.257, 0.261	0.486	_	_
			Total:	1.087, 1.066	0.972	_	_
Rb <sub>2</sub> AgI <sub>3</sub>	0.960	1.055, 1.071	Ag-only:	0.249, 0.265	0.446	_	_
- 0 -			Total:	1.085, 1.056	0.945	_	_
CsAgCl <sub>2</sub>	1.005	0.961	Ag-only:	0.306	_	_	0.699
0 -			Total:	0.965	_	_	1.001
Cs <sub>2</sub> AgCl <sub>3</sub>	0.757	1.155, 1.314	Ag-only:	0.063, 0.236	0.458	_	_
			Total:	1.200, 1.027	0.999	_	_
CsAgBr <sub>2</sub>	1.019	0.968	Ag-only:	0.320	_	_	0.480
			Total:	0.963	_	_	1.024
Cs <sub>2</sub> AgBr <sub>3</sub>	0.980	1.065, 1.096	Ag-only:	0.255, 0.276	0.448	_	_
			Total:	1.066, 1.060	1.016	_	_
$Cs_2AgI_3$	1.004	1.061, 1.177	Ag-only:	0.242, 0.274	0.441	_	_
			Total:	1.103, 1.076	1.016	_	_
$CsAg_2I_3$	0.957	0.859	Ag-only:	_	0.528,  0.666	_	0.814
			Total:	_	0.933, 0.950	_	0.983
CH <sub>3</sub> NH <sub>3</sub> AgBr <sub>2</sub>	0.985	_	Ag-only:	0.290	_	0.695	_
			Total:	Undefined	_	Undefined	_
$CH_3NH_3Ag_2I_3$	0.966	_	Ag-only:	_	0.549, 0.551	_	0.832
			Total:	_	Undefined	_	Undefined

## CH<sub>3</sub>NH<sub>3</sub>AgBr<sub>2</sub>



# CH<sub>3</sub>NH<sub>3</sub>Ag<sub>2</sub>I<sub>3</sub>

Fig. 8 Visualization of the hydrogen bonding in CH<sub>3</sub>NH<sub>3</sub>AgBr<sub>2</sub> (top) and CH<sub>3</sub>NH<sub>3</sub>Ag<sub>2</sub>I<sub>3</sub> (bottom). Bromide ions are shown in brown, iodide ions are shown in purple, silver ions in silver, nitrogen atoms in pale blue, carbon atoms in black, and hydrogens in white.

halide ions are quite different for large spherical ions like Rb<sup>+</sup> and Cs<sup>+</sup> than they are for the methylammonium cation, where hydrogen bonding interactions are stronger and more directional than the ionic bonds between alkali metal cations and halide anions.

It has been suggested by Cheetham et al. that an H-I distance ≤3 Å indicates a hydrogen bonding interaction in the (CH<sub>3</sub>NH<sub>3</sub>)PbI<sub>3</sub> system.<sup>37</sup> Given the smaller radius of the bromide ion (1.82 Å vs. 2.06 Å for 6-coordinate halides)<sup>38</sup> H-Br interactions will be shorter than H-I. Using these descriptors as guidelines, we can determine the number and distances of NH-X interactions in the two crystal structures as shown in Fig. 8. The disorder of the hydrogen atoms in the experimental crystal structures complicates the analysis, however, we can visualize this disordered arrangement as a statistical mixture of two different ordered configurations, each with a staggered conformation of the CH<sub>3</sub>NH<sub>3</sub><sup>+</sup> ion. In the single crystal structures, the hydrogens are split over two sets of equivalent sites, each with 50% occupancy, one of which is shown in Fig. 8. The hydrogen bond distances are the same for both configurations.

The hydrogen bond lengths in each compound are listed in Table 3. Since the bond lengths are the same for each respective

configuration of the CH<sub>3</sub>NH<sub>3</sub><sup>+</sup> ions, only one set is given. The halides with fewer bonds to Ag have shorter NH-X interactions, while the halides with more bonds to Ag have significantly longer NH-X interactions. As the number of Ag atoms coordinating to the halide ion goes up, the need to form substantial hydrogen bonding interactions with CH<sub>3</sub>NH<sub>3</sub><sup>+</sup> cations goes down. For example, the terminal bromide in CH3NH3AgBr2 has a Ag-only BVS of 0.290, indicating it needs significant hydrogen bonding. As a result this bromide has four NH-X interactions between 2.5 and 2.8 Å, which fall into the hydrogen bonding regime. In contrast, the halide site that is threecoordinate with silver has a Ag-only BVS of 0.695, and has only one rather long NH-X interaction with a distance of 3.2826(8) Å. Similar effects are observed in CH3NH3Ag2I3 where the twocoordinate iodides have NH-I interactions near 3 Å, while the four-coordinate iodide has no significant hydrogen bonding interactions. Interestingly, the two crystallographically distinct 2-coordinate iodides in this structure form different numbers of hydrogen bonds. One has three NH-I bonds, all close to  $\sim$  3 Å, while the other appears to form only one hydrogen bond (also  $\sim 3$  Å). The reasons for this asymmetry are not understood at this time.

An interesting result from the crystal chemistry summarized in Table 1 is the overwhelming preference of silver for tetrahedral coordination when the halide is iodide, as opposed to the varied coordination number (4-6) observed in the chloride and bromide systems. 32,39 There are several examples of octahedral [AgCl<sub>6</sub>]<sup>5-</sup> and [AgBr<sub>6</sub>]<sup>5-</sup>, including AgCl and AgBr, both of which adopt the rock salt structure, and the chloride and bromide double perovskites. In contrast, silver is coordinated with six iodide ions at room temperature only in a couple of rare cases. The layered Ruddlesden-Popper family has examples of [AgI<sub>6</sub>]<sup>5-</sup> polyhedra where there are two short and four long bonds. The silver coordination in these systems might be described as intermediate between linear and octahedral. 16-18 To the best of our knowledge, the only other examples of a pseudo-regular  $[AgI_6]^{5-}$  octahedra are  $Tl_2AgI_3$  and  $Tl_6Ag_2I_{10}$ . In Tl<sub>2</sub>AgI<sub>3</sub>, there are polyhedra with six equidistant silver iodide bonds.40 However, this structure contains a tetrahedron-octahedron-tetrahedron trimer [Ag<sub>3</sub>I<sub>8</sub>]<sup>5-</sup> and the octahedral site

Table 3 Lengths of hydrogen bonding (NH-X) interactions in CH<sub>3</sub>NH<sub>3</sub>AgBr<sub>2</sub> and CH<sub>3</sub>NH<sub>3</sub>Ag<sub>2</sub>I<sub>3</sub>. There are two crystallographically distinct two-coordinate iodides

Halide coordination number with Ag	Hydrogen bond distance (Å)
CH <sub>3</sub> NH <sub>3</sub> AgBr <sub>2</sub>	
1	2.5015(6)
	2.5216(6)
	2.7377(8)
	2.7903(8)
3	3.2826(8)
CH <sub>3</sub> NH <sub>3</sub> Ag <sub>2</sub> I <sub>3</sub>	
2	2.9595(8)
	3.0548(1)
	3.0709(9)
2	3.0261(1)
4	None

has a very low silver BVS of 0.714, indicating significant underbonding. Tl<sub>6</sub>Ag<sub>2</sub>I<sub>10</sub> has face-sharing silver iodide octahedra that have short Ag-Ag distances (~2.98 Å) and significant polyiodide character. 41 Compounds with substitutional disorder like AgSbI<sub>4</sub> and AgBiI<sub>4</sub> are excluded as it is not possible to accurately describe individual [AgI<sub>6</sub>]<sup>5-</sup> octahedra when there are mixed 1+/3+ cation sites. 42,43

The strong preference for tetrahedral coordination seen in all A-Ag-I (A = Rb<sup>+</sup>, Cs<sup>+</sup>, CH<sub>3</sub>NH<sub>3</sub><sup>+</sup>) phases goes a long way in explaining the dearth of silver containing iodide double perovskites. Nanocrystals of Cs<sub>2</sub>AgBiI<sub>6</sub> have been reported, but bulk samples of this phase have not been reported. 44,45 A literature search turns up only two reports of silver containing iodide double perovskites in the bulk: (CH3NH3)2AgSbI6 and (CH<sub>3</sub>NH<sub>3</sub>)<sub>2</sub>AgBiI<sub>6</sub>. Both compounds are reported to be tetragonal and have band gaps of  $E_g = \sim 1.95$  eV.<sup>12,13</sup> To better understand this apparent exception to the normal crystal chemistry of silver and iodide, we have resynthesized both compounds and analyzed the resulting deep red powders via PXRD. As shown in Fig. S6 (ESI†), the pattern for the compound reported as (CH<sub>3</sub>NH<sub>3</sub>)<sub>2</sub>AgSbI<sub>6</sub> is well fit to a two-phase mixture of CH<sub>3</sub>NH<sub>3</sub>Ag<sub>2</sub>I<sub>3</sub> and (CH<sub>3</sub>NH<sub>3</sub>)<sub>3</sub>Sb<sub>2</sub>I<sub>9</sub>. This assignment is corroborated by the onset of optical absorption in (CH<sub>3</sub>NH<sub>3</sub>)<sub>3</sub>Sb<sub>2</sub>I<sub>9</sub>, which is reported to be 1.93 eV, nearly identical to what is reported for "(CH3NH3)2AgSbI6".46 A similar analysis performed for (CH<sub>3</sub>NH<sub>3</sub>)<sub>2</sub>AgBiI<sub>6</sub> is less conclusive, however the presence of (CH<sub>3</sub>NH<sub>3</sub>)<sub>3</sub>Bi<sub>2</sub>I<sub>9</sub> is clear in the diffraction patterns (Fig. S7, ESI†). The identity of the additional phase(s) could not be unambiguously determined, but there is no evidence for the presence of a double perovskite phase. From these experiments we conclude that (CH<sub>3</sub>NH<sub>3</sub>)<sub>2</sub>AgSbI<sub>6</sub> and (CH<sub>3</sub>NH<sub>3</sub>)<sub>2</sub>AgBiI<sub>6</sub> cannot be made under the synthesis conditions previously reported, 12,13 whether they can be made by other synthesis approaches is difficult to say with absolute certainty.

## Conclusions

Two new methylammonium silver halide compounds, CH3NH3AgBr2 and CH3NH3Ag2I3, have been prepared and characterized. Each can be synthesized by either solid state or solvothermal methods. The two-coordinate bridging iodide ions in CH3NH3Ag2I3 have significant hydrogen bonding interactions with the CH<sub>3</sub>NH<sub>3</sub><sup>+</sup> cation, while the iodides that are coordinated by four silver ions have minimal interactions with methylammonium. The crystal and electronic structures of CH3NH3Ag2I3 are similar to its all-inorganic analogue, CsAg<sub>2</sub>I<sub>3</sub>, both have a pseudo-one-dimensional character and a band gap of approximately 3.3 eV. In contrast, CH<sub>3</sub>NH<sub>3</sub>AgBr<sub>2</sub> is not isostructural with CsAgBr<sub>2</sub>. The Ag<sup>+</sup> ions adopt tetrahedral coordination in the former and distorted square pyramidal coordination in the latter. In CH<sub>3</sub>NH<sub>3</sub>AgBr<sub>2</sub>, one bromide ion forms a single bond to silver, while the other bromide ion forms three bonds to silver. The one-coordinate bromide ion has significant hydrogen bonding interactions with four neighboring CH3NH3+ groups, while the

three-coordinate bromide does not participate in hydrogen bonding to any appreciable extent. The band gap of CH3NH3AgBr2 is 4.0 eV and the band structure consists of moderately disperse conduction bands with Ag 5s character and flat valence bands that are largely Br 4p in character with some contribution from the Ag 4d orbitals. The ubiquity of tetrahedral coordination for silver, particularly in the ternary iodide compositions discussed here, helps to explain the lack of double perovskite iodides containing Ag<sup>+</sup> cations.

## **Author contributions**

The manuscript was written through contributions of all authors. All authors have given approval to the final version of the manuscript. M. B. Gray conceived of the project, performed syntheses, analyzed crystallographic data, and wrote the initial version of the manuscript. N. P. Holzapfel performed DFT calculation, conducted literature analysis, and computed bond valence sums. T. Liu collected and analyzed single crystal data. V. P. Barbosa collected and analyzed TGA data. N. P. Harvey performed initial syntheses and conducted literature analysis. P. M. Woodward supervised the work and sourced funding.

## Conflicts of interest

The authors declare no competing financial interest.

## Acknowledgements

Funding was provided by the National Science Foundation under award number DMR-2003793. V. P. B. acknowledges support from the Center for Emergent Materials, an NSF MRSEC, under Award DMR-2011876. Special thanks to Anpu Wang for assistance with TGA measurements, to Dr Curtis Moore for assistance with single crystal X-ray diffraction measurements, and to the 11 B-M beamline staff for collection of synchrotron X-ray diffraction measurements. Use of the Advanced Photon Source at Argonne National Laboratory was supported by the U.S. Department of Energy, Office of Science, Office of Basic Energy Sciences, under Contract No. DE-AC02-06CH11357.

## References

- 1 NREL, Best Research-Cell Efficiency Chart. https://www.nrel. gov/pv/cell-efficiency.html (accessed Jan 14, 2021).
- 2 M. B. Gray, J. D. Majher, T. A. Strom and P. M. Woodward, Broadband White Emission in Cs<sub>2</sub>AgIn<sub>1-x</sub>Bi<sub>x</sub>Cl<sub>6</sub> Phosphors, Inorg. Chem., 2019, 58, 13403-13410.
- 3 J. D. Majher, M. B. Gray, T. Amanda Strom and P. M. Woodward, Cs<sub>2</sub>NaBiCl<sub>6</sub>:Mn<sup>2+</sup>: A New Orange-Red Halide Double Perovskite Phosphor, Chem. Mater., 2019, 31, 1738-1744.

- 4 A. H. Slavney, B. A. Connor, L. Leppertb and H. I. Karunadasa, A Pencil-and-Paper Method for Elucidating Halide Double Perovskite Band Structures, Chem. Sci., 2019, 10, 11041-11053.
- 5 W. Meng, X. Wang, Z. Xiao, J. Wang, D. B. Mitzi and Y. Yan, Parity-Forbidden Transitions and Their Impact on the Optical Absorption Properties of Lead-Free Metal Halide Perovskites and Double Perovskites, J. Phys. Chem. Lett., 2017, 8, 2999-3007.
- 6 K.-Z. Du, X. Wang, Q. Han, Y. Yan and D. B. Mitzi, Heterovalent B-Site Co-Alloying Approach for Halide Perovskite Bandgap Engineering, ACS Energy Lett., 2017, 2, 2486-2490.
- 7 E. T. McClure, M. R. Ball, W. Windl and P. M. Woodward, Cs<sub>2</sub>AgBiX<sub>6</sub> (X = Br, Cl): New Visible Light Absorbing, Lead-Free Halide Perovskite Semiconductors, Chem. Mater., 2016, 28, 1348-1354.
- 8 A. H. Slavney, T. Hu, A. M. Lindenberg and H. I. Karunadasa, A Bismuth-Halide Double Perovskite with Long Carrier Recombination Lifetime for Photovoltaic Applications, J. Am. Chem. Soc., 2016, 138, 2138-2141.
- 9 F. Wei, Z. Deng, S. Sun, N. T. P. Hartono, H. L. Seng, T. Buonassisi, P. D. Bristowe and A. K. Cheetham, Enhanced Visible Light Absorption for Lead-Free Double Perovskite Cs<sub>2</sub>AgSbBr<sub>6</sub>, Chem. Commun., 2019, **55**, 3721–3724.
- 10 A. H. Slavney, L. Leppert, A. Saldivar Valdes, D. Bartesaghi, T. J. Savenije, J. B. Neaton and H. I. Karunadasa, Small-Band-Gap Halide Double Perovskites, Angew. Chem., Int. Ed., 2018, 57, 12765-12770.
- 11 F. Wei, Z. Deng, S. Sun, F. Zhang, D. M. Evans, G. Kieslich, S. Tominaka, M. A. Carpenter, J. Zhang, P. D. Bristowe and A. K. Cheetham, Synthesis and Properties of a Lead-Free Hybrid Double Perovskite: (CH<sub>3</sub>NH<sub>3</sub>)<sub>2</sub>AgBiBr<sub>6</sub>, Chem. Mater., 2017, 29, 1089-1094.
- 12 P. Cheng, T. Wu, Y. Li, L. Jiang, W. Deng and K. Han, Combining Theory and Experiment in the Design of a Lead-Free ((CH<sub>3</sub>NH<sub>3</sub>)<sub>2</sub>AgBiI<sub>6</sub>) Double Perovskite, New J. Chem., 2017, 41, 9598-9601.
- 13 Y.-J. Li, T. Wu, L. Sun, R.-X. Yang, L. Jiang, P.-F. Cheng, Q.-Q. Hao, T.-J. Wang, R.-F. Lu and W.-Q. Deng, Lead-Free and Stable Antimony-Silver-Halide Double Perovskite (CH<sub>3</sub>NH<sub>3</sub>)<sub>2</sub>AgSbI<sub>6</sub>, RSC Adv., 2017, 7, 35175–35180.
- 14 T. T. Tran, M. A. Quintero, K. E. Arpino, Z. A. Kelly, J. R. Panella, X. Wang and T. M. McQueen, Chemically Controlled Crystal Growth of (CH<sub>3</sub>NH<sub>3</sub>)<sub>2</sub>AgInBr<sub>6</sub>, CrystEng-Comm, 2018, 20, 5929-5934.
- 15 Z. Deng, F. Wei, S. Sun, G. Kieslich, A. K. Cheetham and P. D. Bristowe, Exploring the Properties of Lead-Free Hybrid Double Perovskites Using a Combined Computational-Experimental Approach, J. Mater. Chem. A, 2016, 4, 12025-12029.
- 16 L.-Y. Bi, Y.-Q. Hu, M.-Q. Li, T.-L. Hu, H.-L. Zhang, X.-T. Yin, W.-X. Que, M. S. Lassoued and Y.-Z. Zheng, Two-Dimensional Lead-Free Iodide-Based Hybrid Double Perovskites: Crystal Growth, Thin-Film Preparation and Photocurrent Responses, J. Mater. Chem. A, 2019, 7, 19662-19667.

- 17 Y. Yao, B. Kou, Y. Peng, Z. Wu, L. Li, S. Wang, X. Zhang, X. Liu and J. Luo, (C<sub>3</sub>H<sub>9</sub>NI)<sub>4</sub>AgBiI<sub>8</sub>: A Direct-Bandgap Layered Double Perovskite Based on a Short-Chain Spacer Cation for Light Absorption, Chem. Commun., 2020, 56, 3206-3209.
- 18 C. Wang, H. Li, M. Li, Y. Cui, X. Son, Q. Wang, J. Jiang, M. Hua, Q. Xu, K. Zhao, H.-Y. Ye and Y. Zhang, Centimeter-Sized Single Crystals of Two-Dimensional Hybrid Iodide Double Perovskite (4,4-Difluoropiperidinium)<sub>4</sub>AgBiI<sub>8</sub> for High-Temperature Ferroelectricity and Efficient X-Ray Detection, Adv. Funct. Mater., 2021, 2009457.
- 19 M. K. Jana, S. M. Janke, D. J. Dirkes, S. Dovletgeldi, C. Liu, X. Qin, K. Gundogdu, W. You, V. Blum and D. B. Mitzi, A Direct-Bandgap 2D Silver-Bismuth Iodide Double Perovskite: The Structure-Directing Influence of an Oligothiophene Spacer Cation, J. Am. Chem. Soc., 2019, 141, 7955-7964.
- 20 A. Cohelo, TOPAS-Academic, Powder Diffr., 2007, 312-317.
- 21 K. Momma and F. Izumi, VESTA 3 for Three-Dimensional Visualization of Crystal, Volumetric and Morphology Data, J. Appl. Crystallogr., 2011, 44, 1272-1276.
- 22 G. M. Sheldrick, SHELXT Integrated Space-Group and Crystalstructure Determination, Acta Crystallogr., Sect. A: Found. Adv., 2015, 71, 3-8.
- 23 G. M. Sheldrick, Crystal Structure Refinement with SHELXL, Acta Crystallogr., Sect. C: Struct. Chem., 2015, 71, 3-8.
- 24 P. Giannozzi, S. Baroni, N. Bonini, M. Calandra, R. Car, C. Cavazzoni, D. Ceresoli, G. L. Chiarotti, M. Cococcioni and I. Dabo, et al., QUANTUM ESPRESSO: A Modular and Open-Source Software Project for Quantum Simulations of Materials, J. Phys.: Condens. Matter, 2009, 21(39), 395502.
- 25 P. Giannozzi, O. Andreussi, T. Brumme, O. Bunau, M. Buongiorno Nardelli, M. Calandra, R. Car, C. Cavazzoni, D. Ceresoli and M. Cococcioni, et al., Advanced Capabilities for Materials Modelling with Quantum ESPRESSO, J. Phys.: Condens. Matter, 2017, 29, 465901.
- 26 BURAI 1.3 A GUI of Quantum ESPRESSO. https://nisihara. wixsite.com/burai (accessed Nov 11, 2020).
- 27 J. P. Perdew, K. Burke and M. Ernzerhof, Generalized Gradient Approximation Made Simple, Phys. Rev. Lett., 1996, 77, 3865-3868.
- 28 H. J. Monkhorst and J. D. Pack, Special Points for Brillouin-Zone Integrations, Phys. Rev. B: Condens. Matter Mater. Phys., 1976, 13, 5188-5192.
- 29 P. Kubelka and F. Munk, The Kubelka-Munk Theory of Reflectance, Z. Tech. Phys., 1931, 591.
- 30 P. Borlido, J. Schmidt, A. Huran, F. Tran, M. Marques and S. Botti, Exchange-Correlation Functionals for Band Gaps of Solids: Benchmark, Reparametrizaiton and Machine Learning, npj Comput. Mater., 2020, 6, 96.
- 31 C. Hasselgren and S. Jagner, Dirubidium Catenapoly[Dichloroargentate(I)-μ-chloro], Acta Crystallogr., 2007, C55, 1208-1210.
- 32 S. Hull and P. Berastegui, Crystal Structures and Ionic Conductivities of Ternary Derivatives of the Silver and Copper Monohalides-II: Ordered Phases within the

- $(AgX)_x$ - $(MX)_{1-x}$  and  $(CuX)_x$ - $(MX)_{1-x}$  (M = K, Rb, and Cs;X = Cl, Br, and I) Systems, J. Solid State Chem., 2004, 177, 3156-3173.
- 33 T. D. Creason, T. M. McWhorter, Z. Bell, M. H. Du and B. Saparov, K<sub>2</sub>CuX<sub>3</sub> (X = Cl, Br): All-Inorganic Lead-Free Blue Emitters with Near-Unity Photoluminescence Quantum Yield, Chem. Mater., 2020, 32, 6197-6205.
- 34 T. D. Creason, A. Yangui, R. Roccanova, A. Strom, M. H. Du and B. Saparov, Rb<sub>2</sub>CuX<sub>3</sub> (X = Cl, Br): 1D All-Inorganic Copper Halides with Ultrabright Blue Emission and Up-Conversion Photoluminescence, Adv. Opt. Mater., 2020, 8, 1901338.
- 35 A. A. Petrov, V. N. Khrustalev, Y. V. Zubavichus, P. V. Dorovatovskii, E. A. Goodilin and A. B. Tarasov, Synthesis and Crystal Structure of a New Hybrid Methylammonium Iodocuprate, Mendeleev Commun., 2018, 28, 245-247.
- 36 N. E. Brese and M. O'Keeffe, Bond-Valence Parameters for Solids, Acta Crystallogr., Sect. B: Struct. Sci., 1991, 47, 192-197.
- 37 J. H. Lee, N. C. Bristowe, P. D. Bristowe and A. K. Cheetham, Role of Hydrogen-Bonding and Its Interplay with Octahedral Tilting in CH<sub>3</sub>NH<sub>3</sub>PbI<sub>3</sub>, Chem. Commun., 2015, 51, 6434-6437.
- 38 R. D. Shannon, Revised Effective Ionic Radii and Systematic Studies of Interatomic Distances in Halides and Chalcogenides, Acta Crystallogr., Sect. A: Cryst. Phys., Diffr., Theor. Gen. Crystallogr., 1976, 32, 751-767.
- 39 M. B. Gray, E. T. McClure and P. M. Woodward, Cs<sub>2</sub>AgBiBr<sub>6-x</sub>Cl<sub>x</sub> Solid Solutions-Band Gap Engineering with Halide Double Perovskites, J. Mater. Chem. C, 2019, 7, 9686-9689.

- 40 M. Hoyer and H. Hartl, Crystal Structure Investigations of TI<sub>2</sub>AgI<sub>3</sub> and NaAgI<sub>2</sub>·3H<sub>2</sub>O, Z. Anorg. Allg. Chem., 1996, **622**, 308-312
- 41 W. Stoeger and A. Rabenau, Tl<sub>6</sub>Ag<sub>2</sub>I<sub>10</sub>, a Polyiodide with Ag<sub>2</sub> Pairs Preparation, Properties, and Crystal Structure, Z. Naturforsch., 1978, 33b, 740-744.
- 42 M. B. Gray, E. T. McClure, N. P. Holzapfel, F. P. Evaristo, W. Windl and P. M. Woodward, Exploring the AgSb<sub>1-x</sub>Bi<sub>x</sub>I<sub>4</sub> Phase Diagram: Thermochromism in Layered CdCl2-Type Semiconductors, J. Solid State Chem., 2021, 121997.
- 43 H. C. Sansom, G. F. S. Whitehead, M. S. Dyer, M. Zanella, T. D. Manning, M. J. Pitcher, T. J. Whittles, V. R. Dhanak, J. Alaria, J. B. Claridge and M. J. Rosseinsky, AgBiI<sub>4</sub> as a Lead-Free Solar Absorber with Potential Application in Photovoltaics, Chem. Mater., 2017, 29, 1538-1549.
- 44 S. E. Creutz, E. N. Crites, M. C. De Siena and D. R. Gamelin, Colloidal Nanocrystals of Lead-Free Double-Perovskite (Elpasolite) Semiconductors: Synthesis and Anion Exchange To Access New Materials, Nano Lett., 2018, 18, 1118-1123.
- 45 B. Yang, J. Chen, S. Yang, F. Hong, L. Sun, P. Han, T. Pullerits, W. Deng and K. Han, Lead-Free Silver-Bismuth Halide Double Perovskite Nanocrystals, Angew. Chem., Int. Ed., 2018, 57, 5359-5363.
- 46 D. Ju, X. Jiang, H. Xiao, X. Chen, X. Hu and X. Tao, Narrow Band Gap and High Mobility of Lead-Free Perovskite Single Crystal Sn-Doped MA<sub>3</sub>Sb<sub>2</sub>I<sub>9</sub>, J. Mater. Chem. A, 2018, 6, 20753-20759.